A New Method to Dynamically Measure the Surface Tension, Viscosity, and Density of Melts

STEVEN J. ROACH and HANI HENEIN

A new formulation has been developed to describe the fluid dynamics of a liquid draining through an orifice under the influence of gravity. The model relates experimental quantities of head and flow rate, with surface tension, viscosity, and density, facilitating the calculation of all three properties. Experiments performed with molten aluminum at temperatures from 937 to 1173 K indicate that surface tension (N/m) and density (kg/m^3) are [$0.871 - 0.155 \times 10^{-3} (T - T_{liq})$] and [$2390 - 0.15 (T - T_{liq})$], which is within 6.5 and 2.5 pct, respectively, of values reported in the literature. The viscosity has been determined to be 5.2×10^{-4} Nsm^{-2}, which is significantly less than data reported from other sources. The method is unique because the measurements are performed under highly dynamic conditions.

I. INTRODUCTION

KNOWLEDGE of the physical properties of melts is fundamentally important for many metallurgical processes. The term "melt" refers to molten materials such as metals, salts, slags, *etc*. The productivity and efficiency of many high-temperature applications rely on accurate knowledge of surface tension, viscosity, and density of the melt under consideration. This article will introduce a method that simultaneously calculates all three properties using one experimental setup.

Density is required in studies ranging from simple mass balance calculations to the study of natural convection. Other examples include predicting the separation of slag/metal systems or calculating the terminal velocity of inclusions within a melt. Density is also required to quantify other physical properties such as surface tension and dynamic viscosity.

Viscosity is a quantity of fundamental importance in fluid transport problems, as well as in issues concerning reaction kinetics in melt processing. The viscosity of molten systems often dictates the castability (or ability to fill a mold cavity) of many metals and their alloys.[1] Furthermore, the mechanisms of solidification often require knowledge of the viscosity of the melt.[2,3]

Surface tension is a significant property in atomization and granulation studies for the powder metallurgy industry, because the efficiency of these processes is directly related to the surface tension of the melt.[4] The Marangoni effect has been discussed extensively in the literature and describes convection induced within a liquid from gradients in surface tension. In welding, penetration of the liquid phase is dependent on this phenomenon.[5] The Marangoni effect also plays a crucial role in the corrosion of refractory material at slag-gas and slag-metal interfaces. The rate of nitrogen absorption in iron is also dependent on this phenomenon in steelmaking.[6]

In order to manipulate metallurgical processes, a complete database of these properties should be available. Unfortunately, there is much work that needs to be done in applying property data to many processing environments. Many of the techniques used in measuring physical properties of low-temperature liquids (water, organic liquids) are not applicable for melts because of a number of factors. Material selection at high temperatures, temperature control and monitoring, and other issues constrain measuring techniques considerably. The reactive nature that molten metals exhibit with oxygen is problematic and great lengths have been made to provide an inert atmosphere for experimentation. In measuring surface tension, contamination has a particularly drastic impact on the surface tension of molten metals. Oxide accumulation has been known to affect the surface tension of these liquids in the presence of very low levels of oxygen.[5,7,8] To further complicate matters, methods used to measure the surface tension of melts are predominantly static, providing an opportunity for contaminants to accumulate.

In this study, a new technique will be introduced that simultaneously measures the surface tension, viscosity, and density of melts. This method relies on formulations that describe flow through an orifice under the influence of gravity. Results with molten aluminum will be presented and compared with data available in the literature. This method is unique since it is performed in a highly dynamic manner. Numerous measurements are made during the course of one experiment because experimental variables change as the vessel drains, thereby giving this new method significant advantages over conventional techniques.

II. FORMULATION

In a previous contribution, a new formulation was developed that includes potential, kinetic, and surface forces to describe the fluid dynamics of stream flowing from an orifice under the influence of gravity[9,10] (refer to Figure 1 for a schematic of the system). The derivation is similar to the traditional Bernoulli formulation ($Q = \pi r_o^2 \sqrt{2gh}$) except that an additional term is included because pressure

STEVEN J. ROACH is with INCO Ltd., Ontario Division, CCNR Technical Services, Copper Cliff, ON, Canada P0M 1N0. HANI HENEIN, Professor and Director, is with the Advanced Materials and Processing Laboratory, Department of Chemical and Materials Engineering, University of Alberta, Edmonton, AB, Canada T6G 2G6. Contact e-mail: hani.henein@ualberta.ca

Manuscript submitted June 26, 2003.

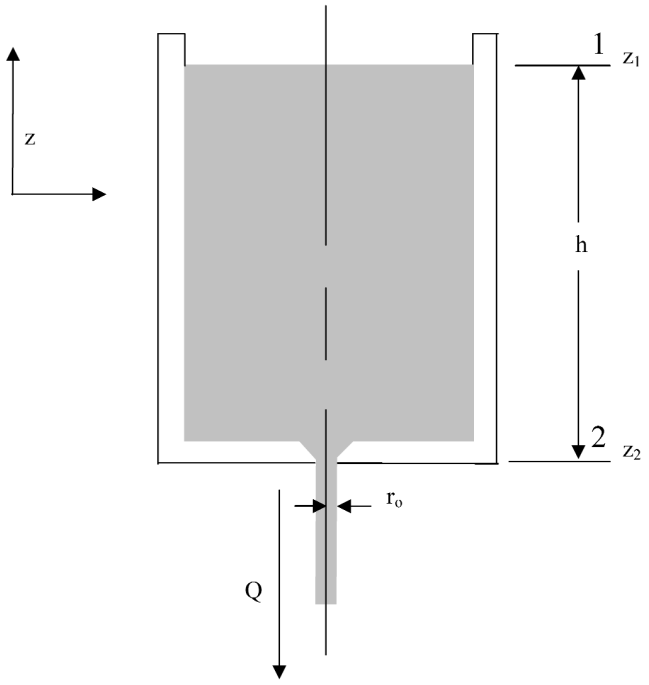

Fig. 1—Schematic of draining vessel system depicting flow rate of a fluid through an orifice.

induced from surface tension is quantified in the model. In terms of volumetric flow rate, the expression is written as

$$Q = \pi r_o^2 C_d \sqrt{2g\left(h - \frac{\sigma}{\rho g r_o}\right)} \quad [1]$$

or, in dimensionless form,

$$\mathrm{Fr} + \mathrm{Bo}^{-1} = 1 \quad [2]$$

where Fr is the Froude number, given by

$$\mathrm{Fr} = \frac{\left(\frac{Q}{\pi r_o^2 C_d}\right)^2}{2gh} \quad [3]$$

and Bo is the Bond number, given by

$$\mathrm{Bo} = \frac{\rho g r h}{\sigma} \quad [4]$$

The Froude number represents the ratio of the inertial force of the stream to the potential force of the liquid head above the orifice discharge. The Bond number represents the ratio of the potential force to the surface force of the stream exiting the orifice (induced by the liquid surface tension).

The discharge coefficient, C_d, accounts for frictional losses in the orifice and is a function of the Reynolds number given in terms of the experimental volumetric flow rate as follows:

$$\mathrm{Re} = \frac{2\rho Q_{\exp}}{\pi r_o \eta} \quad [5]$$

Using liquids of known physical properties and the orifice to be used with melts, a calibration of C_d *vs* Re may be developed.[9,10] Water was used as a calibration fluid; the results

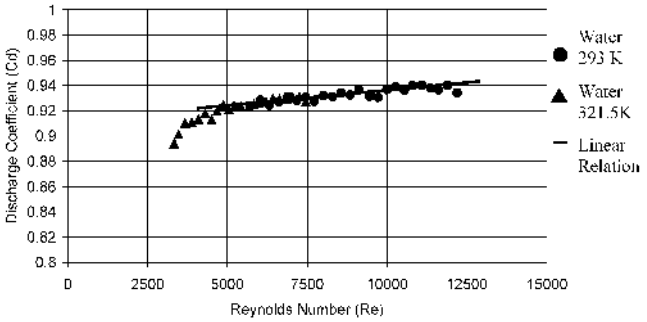

Fig. 2—Frictional characteristics of the 0.005-m- (5-mm-) diameter orifice.

for two separate calibrations are presented in Figure 2. For $4000 > \mathrm{Re} > 13{,}000$, the relationship may be expressed as

$$C_d = a(\mathrm{Re}) + b = 2.196 \times 10^{-6}(\mathrm{Re}) + 0.914 \quad [6]$$

Equations [1] and [5] or [2] through [5], as well as the C_d *vs* Re calibration given by Eq. [6], are used to determine the properties of melts.

Experimental measurements of head and flow rate are made as a liquid drains through an orifice. Such data will be used in the model to simultaneously calculate surface tension, viscosity, and density using the Gauss–Newton method for nonlinear regression analysis.

By rearranging Eq. [1], the experimental head can be expressed as a function of experimental volumetric flow rate:

$$h_{\exp} = \frac{1}{2g}\left(\frac{Q_{\exp}}{C_d \pi r_o^2}\right)^2 + \frac{\sigma}{\rho g r_o} + \delta h_{\exp} \quad [7]$$

The quantity $\delta h_{\exp}$ represents the error between experimental and calculated head measurements. Assuming a linear relationship between Reynolds number and discharge coefficient (Eq. [6] and Figure 2), Eq. [7] can be expressed in terms of linear constants a and b, as follows:

$$h_{\exp} = \frac{1}{2g}\left(\frac{Q_{\exp}}{\left(a\left(\frac{2\rho r_o Q_{\exp}}{\pi r_o^2 \eta}\right) + b\right)\pi r_o^2}\right)^2 + \frac{\sigma}{\rho g r_o} + \delta h_{\exp} \quad [8]$$

Since it is cumulative mass data that is generated as the vessel drains and density is unknown, mass flux, $V_{\exp}$, is introduced to replace $Q_{\exp}$:

$$V_{\exp} = \frac{\rho Q_{\exp}}{\pi r_o^2} \quad [9]$$

Equation [7] is now expressed as follows:

$$h_{\exp} = f(V_{\exp}) + \delta h_{\exp} = \frac{1}{2g}\left(\frac{V_{\exp}}{\rho\left(a\left(\frac{2r_o V_{\exp}}{\eta}\right) + b\right)}\right)^2 + \frac{\sigma}{\rho g r_o} + \delta h_{\exp} \quad [10]$$

A linear approximation of theoretical head can be performed using a Taylor series expansion around unknown properties, σ, η, and ρ.

$$f(V_{\text{exp}})_{j+1} = f(V_{\text{exp}})_j + \frac{\partial f(V_{\text{exp}})_j}{\partial \sigma}\Delta\sigma + \frac{\partial f(V_{\text{exp}})_j}{\partial \eta}\Delta\eta + \frac{\partial f(V_{\text{exp}})_j}{\partial \rho}\Delta\rho \quad [11]$$

where subscript $j+1$ refers to updated values after a single iteration of the algorithm. In applying the Taylor series approximation to predict theoretical head, Eq. [10] can be written as follows:

$$(h_{\text{exp}})_j = f(V_{\text{exp}})_{j+1} + (\delta h_{\text{exp}})_j \quad [12]$$

Substituting Eq. [11] into Eq. [12],

$$(h_{\text{exp}})_j - f(V_{\text{exp}})_j = \frac{\partial f(V_{\text{exp}})_j}{\partial \sigma}\Delta\sigma + \frac{\partial f(V_{\text{exp}})_j}{\partial \eta}\Delta\eta + \frac{\partial f(V_{\text{exp}})_j}{\partial \rho}\Delta\rho + (\delta h_{\text{exp}})_j \quad [13]$$

As the vessel drains, experimental head and mass flux can be written in vector notation:

$$h_{\text{exp}} = \begin{bmatrix} h_{1,\text{exp}} \\ \cdot \\ \cdot \\ h_{i,\text{exp}} \\ h_{n,\text{exp}} \end{bmatrix} \quad [14]$$

$$V_{\text{exp}} = \begin{bmatrix} V_{1,\text{exp}} \\ \cdot \\ \cdot \\ V_{i,\text{exp}} \\ V_{n,\text{exp}} \end{bmatrix} \quad [15]$$

Equation [13] can be written as

$$\{Y\} = [Z]\{\Delta x\} + \{\Delta E\} \quad [16]$$

where $[Z]$ is a matrix of partial derivatives:

$$[Z] = \begin{Bmatrix} \frac{\partial f(V_{1,\text{exp}})}{\partial \sigma} & \frac{\partial f(V_{1,\text{exp}})}{\partial \eta} & \frac{\partial f(V_{1,\text{exp}})}{\partial \rho} \\ \cdot & \cdot & \cdot \\ \cdot & \cdot & \cdot \\ \frac{\partial f(V_{i,\text{exp}})}{\partial \sigma} & \frac{\partial f(V_{i,\text{exp}})}{\partial \eta} & \frac{\partial f(V_{i,\text{exp}})}{\partial \rho} \\ \frac{\partial f(V_{n,\text{exp}})}{\partial \sigma} & \frac{\partial f(V_{n,\text{exp}})}{\partial \eta} & \frac{\partial f(V_{n,\text{exp}})}{\partial \rho} \end{Bmatrix}_j \quad [17]$$

The partial derivatives of Eq. [13] with respect to σ, η, and ρ for each measurement are given in Eqs. [18] through [20]:

$$\frac{\partial f(V_{i,\text{exp}})}{\partial \sigma} = \frac{1}{\rho g r_{\text{o}}} \quad [18]$$

$$\frac{\partial f(V_{i,\text{exp}})}{\partial \eta} = \frac{V_{i,\text{exp}}^2}{g\rho^2}\left(\frac{1}{a\left(\frac{2r_{\text{o}}V_{i,\text{exp}}}{\eta}\right) + b}\right)^3\left(\frac{2ar_{\text{o}}V_{i,\text{exp}}}{\eta^2}\right) \quad [19]$$

$$\frac{\partial f(V_{i,\text{exp}})}{\partial \rho} = -\frac{1}{g\rho^3}\left(\frac{V_{i,\text{exp}}}{\left(a\left(\frac{2r_{\text{o}}V_{i,\text{exp}}}{\eta}\right) + b\right)}\right)^2 - \frac{\sigma}{\rho^2 g r_{\text{o}}} \quad [20]$$

The vector $\{Y\}$ corresponds to the difference between experimental and calculated head values:

$$\{Y\} = \begin{bmatrix} h_{1,\text{exp}} - f(V_{1,\text{exp}}) \\ \cdot \\ \cdot \\ h_{i,\text{exp}} - f(V_{i,\text{exp}}) \\ h_{n,\text{exp}} - f(V_{n,\text{exp}}) \end{bmatrix}_j \quad [21]$$

Vector $\{\Delta x\}$ corresponds to the change in property values after each iteration:

$$\{\Delta x\} = \begin{bmatrix} \Delta\sigma \\ \Delta\eta \\ \Delta\rho \end{bmatrix} \quad [22]$$

The vector, $\{\Delta E\}$, is the error associated with differences between experimental and calculated head values. Applying linear least-squares theory results in the following matrix inverse relationship:

$$\{\Delta x\} = ([Z]^T[Z])^{-1}[Z]^T\{Y\} \quad [23]$$

Updated values for σ, η, and ρ are calculated after each iteration:

$$\sigma_{j+1} = \sigma_j + \Delta\sigma \quad [24]$$

$$\eta_{j+1} = \eta_j + \Delta\eta \quad [25]$$

$$\rho_{j+1} = \rho_j + \Delta\rho \quad [26]$$

Convergence is attained once the following quantities are less than the specified tolerance, ε:

$$\varepsilon_\sigma \geq \frac{\sigma_{j+1} - \sigma_j}{\sigma_{j+1}} \quad [27]$$

$$\varepsilon_\eta \geq \frac{\eta_{j+1} - \eta_j}{\eta_{j+1}} \quad [28]$$

$$\varepsilon_\rho \geq \frac{\rho_{j+1} - \rho_j}{\rho_{j+1}} \quad [29]$$

Once all convergence criteria given by Eqs. [27] through [29] are satisfied, the physical properties of the fluid are the values given by σ_{j+1}, η_{j+1}, and ρ_{j+1}.

Experimental

The experiments were carried out in an inert chamber depicted schematically in Figure 3. Argon is pumped into the unit until a small overpressure is obtained; thus, air does not

leak back into the unit. A continuous purge of argon is run through the unit until a nominal oxygen level of 20 ppm is registered from the oxygen monitor.

Aluminum is placed into a graphite crucible that has a capacity of approximately 1 L (~1.5 kg molten aluminum). An orifice plate constructed of high-density graphite is inserted through the bottom of the crucible and fastened in place. Figure 4 illustrates the dimensions and the geometry of the orifice plate. It is necessary that the outlet diameter of the orifice be known with a high degree of precision. Providing inaccurate values of r_o in the formulation will result in significant systematic errors in the property values of the fluid.

The 99.95 pct purity aluminum used in these experiments was melted using induction heating, and the liquid metal temperature was monitored using a thermocouple immersed into the melt. It is essential to measure the temperature of the melt near the orifice.[9,10] Temperature dependence on physical properties can be significant.[2] The thermocouple is placed vertically in the crucible until it is 1 to 2 mm from the bottom. It is also placed approximately 1 cm to the side so that it does not interfere with the flow characteristics of the melt exiting the crucible.

One of the issues with induction heating is the electromagnetic force that induces movement in the melt. This would alter the calculation since melt movement in the crucible is not considered in the formulation. For this reason, induction heating is turned off once the melt is ready to pour through the orifice. The thermocouple does record a temperature decrease of as much as 20 °C from the start to the end of the melt flow duration for the crucible emptying. The expected error will be less than 1 pct for surface tension and density based on data in the literature.[2,7] For viscosity, however, this temperature decrease may affect the measurement slightly more (~5 pct).[35]

Once the aluminum is molten and the oxygen content in the unit has reached equilibrium, the melt is poured through the orifice plate and onto a loadcell that registers cumulative mass. During heating, a stopper rod covers the bottom of the orifice and is released when the experiment is ready to proceed. To ensure the loadcell is kept sufficiently cool, the melt is captured onto a stainless steel pan containing silica sand, which dissipates heat.

A data acquisition system records signals from the oxygen analyzer, thermocouple, and loadcell. The mass flux is obtained from the cumulative mass, C_m, *vs* time curve recorded by the loadcell (Figure 5). A second-order polynomial curve is fit to the data. A higher order polynomial curve did not improve accuracy. A polynomial fit on a set of data collected for aluminum through a 5-mm-diameter orifice at 1073 K is expressed as

$$C_m = -8.356 \times 10^{-4}(t)^2 + 6.491 \times 10^{-2}(t) + 2.212 \times 10^{-2}\ (\text{kg}) \quad [30]$$

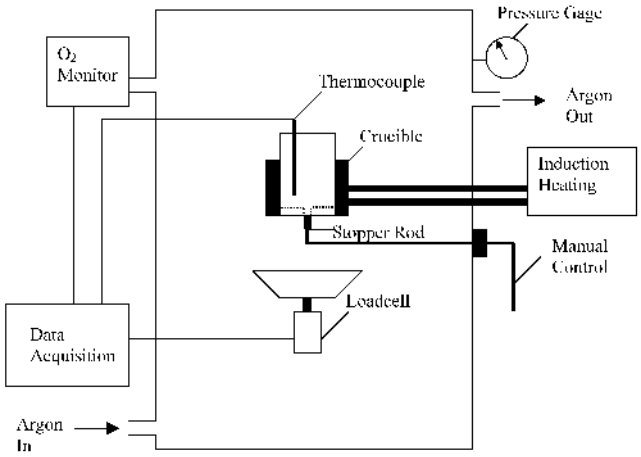

Fig. 3—Experimental apparatus.

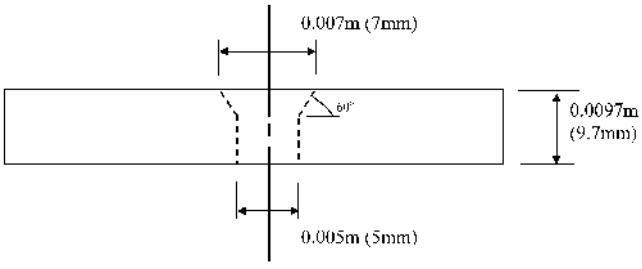

Fig. 4—Orifice plate dimensions.

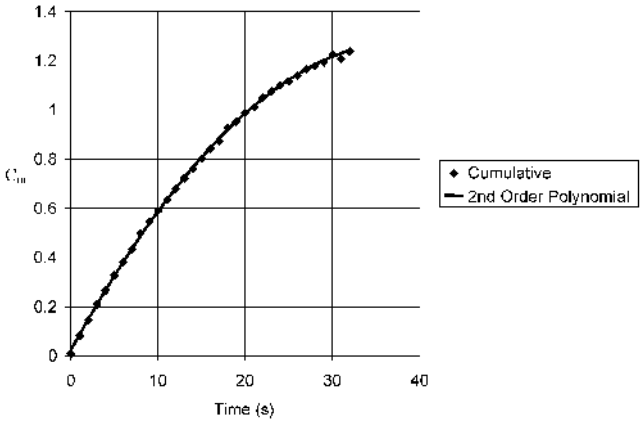

Fig. 5—Cumulative mass *vs* time for aluminum at 1073 K.

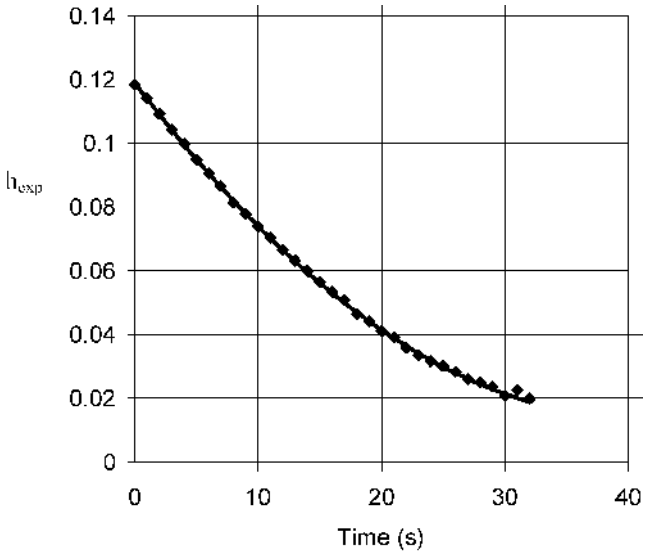

Fig. 6—Experimental head measurements for aluminum at 1073 K.

Differentiating Eq. [30] with respect to time, and dividing by the cross-sectional area of the orifice, provides flux:

$$V_{\text{exp}} = \frac{1}{\pi {r_o}^2}\frac{dC_M}{dt} = -8.52 \times 10^1(t) + 6.491 \times 10^{-2} \quad [31]$$

Head, h_{exp}, is obtained using loadcell information as well. Knowing the geometry of the crucible, head can be determined by monitoring the quantity of material that poured through the orifice as a function of time. The density of the liquid is required for the calculation and was provided from the literature for molten aluminum.[2] This value of density was used to initiate the iteration process and was subsequently updated during the course of the solution, as will be illustrated in Section III. Figure 6 illustrates head as a function of time using this approach.

III. RESULTS: MOLTEN ALUMINUM

Using the multiple nonlinear regression analysis formulation, surface tension, viscosity, and density were determined for a system of aluminum at 1073 K. Results are presented in Table I with values quoted from the literature. The density and surface tension have a percent difference of only 1.2 and 2.5 pct, respectively, with respect to values in the literature. Viscosity, however, was determined to be significantly lower than the values quoted from the literature. Insight into this result will be provided in the discussion of viscosity.

The complication in using known density information in determining head will now be addressed. An iterative approach is taken to calculate the properties using published or an estimated value of density as an initial guess. The new density determined by the model is used in subsequent iterations in the model. This iterative process continues until density does not change appreciably (*i.e.*, converges). The results from this approach are shown in Table II. It is clear that properties rapidly converge. The relative error in density after applying data from Iida and Guthrie is 0.5 pct.[2] This is deemed acceptable for all subsequent head estimations. In the future, alternative means in generating head data will be investigated. An error analysis and the temperature dependence of surface tension, density, and viscosity of aluminum will now be presented.

A. *Surface Tension*

The surface tension of aluminum at 1073 K determined for all head measurements is illustrated in Figure 7. Applying viscosity and density results from the regression, and writing the formulation in terms of surface tension yields

$$\sigma = \rho g r_o \left[h_{\text{exp}} - \frac{1}{2g}\left(\frac{Q_{\text{exp}}}{C_d \pi {r_o}^2}\right)^2 \right] \quad [32]$$

An error analysis can be applied so that the scatter illustrated in Figure 7 can be predicted.

1. *Error analysis*

Errors in head, flow rate, and discharge coefficient will contribute to error in calculating surface tension. Propagation of errors is used to quantify these effects.[11] From the experimental results presented in Figure 7, it appears that errors in head result in random scatter. Only errors in head were quantified; however, formulations including errors in flow rate and discharge coefficient are also included. A full

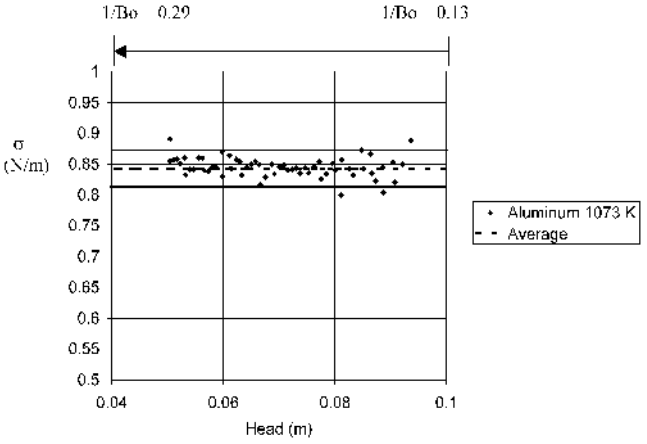

Fig. 7—Surface tension of aluminum determined at 1073 K, with expected error in surface tension due to error in head measurement represented by the solid lines.

Table I. Summary of Regression Results for Aluminum at 1073 K

Surface Tension (N/m)		Viscosity (Nsm^{-2})		Density (kg/m^3)	
Keene[7]	This Study	Rothwell[30]	This Study	Iida and Guthrie[2]	This Study
0.864	0.842 ± 0.020	1.1×10^{-3}	$5.22 \times 10^{-4} \pm 0.35 \times 10^{-4}$	2328	2361 ± 46
Pct diff	2.55 Pct	Pct diff	52.5 Pct	Pct diff	1.23 Pct

Table II. Physical Properties of Aluminum at 1073 K Determined from Regression by Iteratively Updating Density in the Estimation of Head

Property	ρ = 2328 kg/m^2 (Iida and Guthrie[2])	ρ = 2361 kg/m^3 (Second Iteration)	ρ = 2371 kg/m^3 (Third Iteration)
Surface tension (N/m)	0.842 ± 0.020	0.853 ± 0.016	0.850 ± 0.016
Viscosity (Ns/m^2)	$5.22 \times 10^{-4} \pm 0.35 \times 10^{-4}$	$5.26 \times 10^{-4} \pm 0.36 \times 10^{-4}$	$5.18 \times 10^{-4} \pm 0.36 \times 10^{-4}$
Density (kg/m^3)	2361 ± 46	2371 ± 46	2370 ± 46

description of this approach with complete derivations is available elsewhere.[9]

Propagation of errors analysis applied to surface tension is written as follows:

$$\delta\sigma = \sqrt{\left(\frac{\partial\sigma}{\partial h_{\text{exp}}}\right)^2 (\delta h_{\text{exp}})^2 + \left(\frac{\partial\sigma}{\delta Q_{\text{exp}}}\right)^2 (\delta Q_{\text{exp}})^2 + \left(\frac{\partial\sigma}{\partial C_d}\right)^2 (\delta C_d)^2} \quad [33]$$

The value $\delta\sigma$ is the expected deviation in surface tension. Quantities, δh_{exp}, δQ_{exp}, and δC_d represent standard deviations in head, flow rate, and discharge coefficient, respectively.

The differentials in Eq. [33] are determined by taking the derivative of Eq. [32] with respect to h_{exp}, Q_{exp}, and C_d. These relationships are represented in Eqs. [34] through [36]:

$$\frac{\partial\sigma}{\partial h_{\text{exp}}} = \rho g r_{\text{o}} \quad [34]$$

$$\frac{\partial\sigma}{\partial Q_{\text{exp}}} = -\frac{\rho r_{\text{o}}}{C_d \pi {r_{\text{o}}}^2}\left(\frac{Q_{\text{exp}}}{C_d \pi {r_{\text{o}}}^2}\right) \quad [35]$$

$$\frac{\partial\sigma}{\partial C_d} = \frac{\rho r_{\text{o}}}{C_d}\left(\frac{Q_{\text{exp}}}{C_d \pi {r_{\text{o}}}^2}\right)^2 \quad [36]$$

The standard deviation in head was determined to be 0.5×10^{-3} m from repeat experiments.[9] This quantity and the values from Eq. [34] were substituted into Eq. [33]. The solid lines illustrated in Figure 7 represent the predicted deviation in surface tension determined from this approach only based on the error in measuring head. The error analysis predicts scatter in the evaluation of surface tension since the majority of calculations are confined within the predicted boundary. Clearly, the contributions of error due to Q_{exp} and C_d are negligible.

2. *Surface tension of aluminum as a function of temperature*

The surface tension of molten aluminum was measured as a function of temperature between 973 K (700 °C) and 1173 K (900 °C). The results are presented in Figure 8 with values available in the literature. In a thorough review of the surface tension of molten metals, Keene proposed a correlation for the surface tension of aluminum as a function of temperature.[7] He did this by taking the average results of 20 independent studies.[12–29] The function is expressed as follows:

$$\sigma_{\text{Al}} = 0.871 - 0.155 \times 10^{-3}\,(T - T_{\text{liq}}) \quad [37]$$

This relation is illustrated in Figure 8. The melting point of aluminum, T_{liq}, is 933 K (660 °C).

Equation [37] represents the surface tension of oxidized aluminum. Oxide contamination on the surface of aluminum occurs in the presence of even trace amounts of oxygen (partial pressure of oxygen must be $<10^{-39}$ Pa to avoid oxidation of molten aluminum). Kaptay stated that measurements have traditionally been performed in the presence of a layer of supercooled Al_2O_3 on the surface.[8]

Goumiri and Joud[12] determined the surface tension of unoxi dized aluminum by providing strict measures to significantly reduce oxygen content. A combination of heating and cooling and ion bombardment of the surface provided results that were much higher than values obtained from other sources. In Figure 8, the surface tension determined in that study is 21 pct higher than the value obtained by Keene at 973 K (700 °C).

A comparison of the draining vessel method with conventional methods is warranted. Of the 20 studies considered in generating Eq. [37], 8 used the maximum bubble pressure method (MBP) and 12 used the sessile drop method (SD).[7] Goumiri and Joud used the sessile drop method for their analysis.[12] A full description of these methods, as well as other methods used for melts, are available in Iida and Guthrie.[2] Techniques rely on formulations in which potential and surface forces are balanced. For instance, the sessile drop method balances the weight of a droplet resting on a substrate with surface forces that are a function of the shape of the droplet as well as the surface tension of the liquid. The maximum bubble pressure technique measures the pressure of a bubble generated from the tip of a capillary that is submerged a specific depth within the liquid. At the point where the bubble detaches, surface forces overcome both the pressure in the capillary as well as the pressure exerted by the static head of liquid.

The draining vessel approach, in addition to balancing potential and surface forces, accounts for the inertial force of the exiting stream in the formulation, as indicated by the introduction of the Froude number in Eq. [2]. Both MBP and SD methods are static in comparison since the surface of the liquid is stationary during the coarse of the measurement. This poses significant implications for molten metals since these liquids are susceptible to oxide accumulation that can significantly lower surface tension. The maximum bubble pressure method, however, can apply high bubble rates (>0.1 seconds) to minimize exposure time to contaminants.[30]

Results illustrated in Figure 8 are similar in magnitude to those stated by Keene. In Keene's relationship, in each study he examined, the melt appeared to have an oxide layer on the surface, lowering the surface tension of the "pure" melt. Note that the results reported by Goumiri and Joud[12] are higher for an oxide-free surface. Thus, despite the highly dynamic nature in which the draining vessel operates, results suggest that surface tension determined *via* this method, under experimental conditions described earlier, reflects an oxidized state of the aluminum surface. From a validation perspective, however, these results are encouraging since

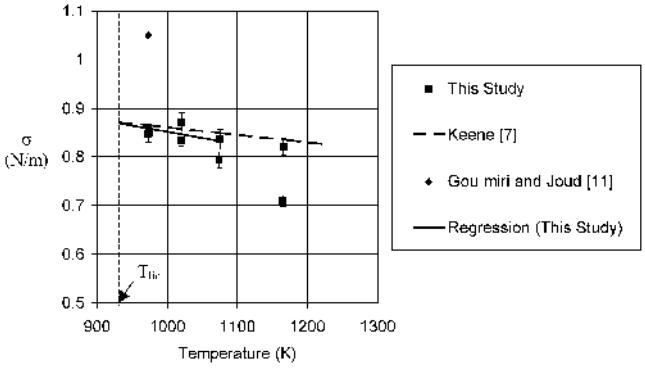

Fig. 8—Surface tension of aluminum as a function of temperature.

Keene's relationship accounts for a number of independent studies.

Referring to Figure 8, it is more difficult to obtain consistent results at higher temperatures. This is attributed to fluctuations in oxygen content at these temperatures. The apparatus could not reliably provide the nominal 20 ppm oxygen content at temperatures above 1073 K (800 °C).[9] A linear relation is proposed and presented in Table III for temperatures between 973 and 1073 K. The difference between this relationship and Keene's formula is no greater than 6.5 pct over this temperature range.

B. *Density*

The density of aluminum at 1073 K for all head measurements is illustrated in Figure 9. Applying surface tension and viscosity results from the regression, and writing the formulation in terms of density, yields

$$\rho = \frac{\sigma}{g r_o \left(h_{exp} - \frac{1}{2g} \left(\frac{Q_{exp}}{C d \pi r_o^2} \right)^2 \right)} \quad [38]$$

Error analysis will be applied to predict the scatter depicted in Figure 9.

1. *Error analysis*

Similar to surface tension and viscosity evaluations, predicted error in density will only consider the standard deviation in head:

Table III. Temperature Dependence of Surface Tension of Aluminum

Source	Surface Tension at Melting Point, σ_{liq} (N/m)	Temperature Dependence of Surface Tension, $d\sigma/dT$ (Nm^{-1} K^{-1})
Keene[7]	0.871	-0.155×10^{-3}
This study	0.868	-0.25×10^{-3}

$\sigma = \sigma_{liq} + d\sigma/dT(T - T_{liq})$

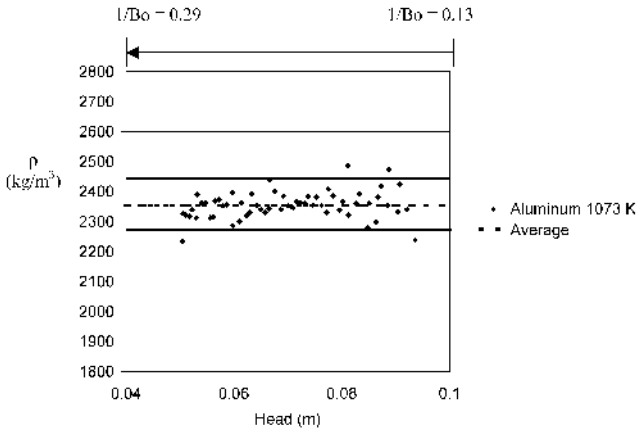

Fig. 9—Density of aluminum determined at 1073 K, with expected error represented by the solid lines.

$$\delta\rho = \sqrt{\left(\frac{\partial\rho}{\partial h}\right)^2 (\delta h)^2 + \left(\frac{\partial\rho}{\partial Q_{exp}}\right)^2 (\delta Q_{exp})^2 + \left(\frac{\partial\rho}{\partial C_d}\right)^2 (\delta C_d)^2} \quad [39]$$

The differentials in Eq. [39] are

$$\frac{\partial\rho}{\partial h} = -\frac{\rho^2 g r_o}{\sigma} \quad [40]$$

$$\frac{\partial\rho}{\partial Q_{exp}} = \frac{\rho^2 Q_{exp}}{C_d^2 \pi^2 r_o^3 \sigma} \quad [41]$$

$$\frac{\partial\rho}{\partial C_d} = -\frac{\rho^2 Q_{exp}^2}{\sigma \pi^2 r_o^3 C_d^3} \quad [42]$$

Refer to the scatter in calculating density from Figure 9. Since calculations are confined to the predicted boundary, error analysis reasonably predicts the error in density.

2. *Density of aluminum as a function of temperature*

Figure 10 presents results for molten aluminum as a function of temperature. The relation quoted by Iida and Guthrie is also included.[2] There appears to be excellent agreement between results obtained *via* the draining vessel method and those quoted in the literature. This provides an important validation of the method.

A complete discussion of measuring the density of melts is available elsewhere; however, measurements are traditionally done in static situations.[2] Proper design and material selection are required to make these measurements at high temperatures.

Table IV presents a function that represents the results depicted in Figure 10. The difference between this function and the one from the literature is no greater than 2.5 pct between 973 K (700 °C) and 1173 K (900 °C).

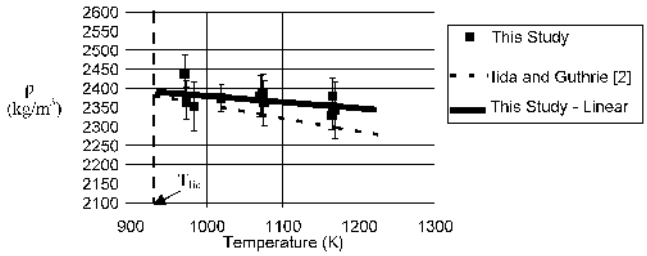

Fig. 10—Density of aluminum as a function of temperature.

Table IV. Temperature Dependence of Density of Aluminum

Source	Density at Melting Point, ρ_{liq} (kg/m^3)	Temperature Dependence of Density, $d\rho/dT$ (kg m^{-3} K^{-1})
Iida and Guthrie[2]	2380	−0.35
This study	2390	−0.15

$\rho = \rho_{liq} + d\rho/dT(T - T_{liq})$

C. *Viscosity*

The viscosity of aluminum at 1073 K determined for all head measurements is illustrated in Figure 11. Applying surface tension and density results from the regression, and writing the formulation in terms of viscosity, yields

$$\eta = \frac{2a\rho r_o Q_{exp}}{\frac{Q_{exp}}{\sqrt{2g\left(h_{exp} - \frac{\sigma}{\rho g r_o}\right)}} - \pi r_o{}^2 b} \qquad [43]$$

Error analysis will be applied to the viscosity measurement.

1. *Error analysis*

Similar to surface tension, $\delta\eta$ is attributed to errors in head (0.5×10^{-3} m); however, errors in flow rate and discharge coefficient will be included in the analysis.

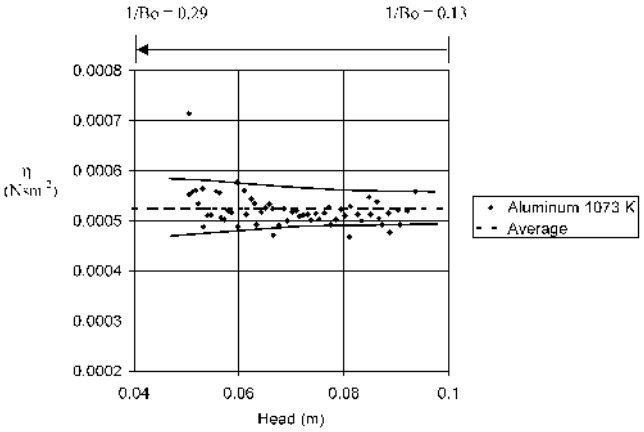

Fig. 11—Viscosity of aluminum determined at 1073 K, with expected error represented by the solid lines.

$$\delta\eta = \sqrt{\left(\frac{\partial\eta}{\partial h_{exp}}\right)^2 (\delta h_{exp})^2 + \left(\frac{\partial\eta}{\partial Q_{exp}}\right)^2 (\delta Q_{exp})^2 + \left(\frac{\partial\eta}{\partial a}\right)^2 (\delta a)^2 + \left(\frac{\partial\eta}{\partial b}\right)^2 (\delta b)^2} \qquad [44]$$

The differentials presented in Eq. [44] are presented in Eqs. [45] through [48]:

$$\frac{\partial\eta}{\partial h_{exp}} = \frac{2a\rho r_o g Q_{exp}{}^2}{\pi^2 r_o{}^4 [C_d - b]^2 \left[2gh\left(1 - \frac{\sigma}{\rho g r_o h_{exp}}\right)\right]^{3/2}} \qquad [45]$$

$$\frac{\partial\eta}{\partial Q_{exp}} = -\frac{2a\rho d}{\pi r_o (C_d - b)^2} \qquad [46]$$

$$\frac{\partial\eta}{\partial a} = \frac{2\rho r_o Q_{exp}}{\pi r_o{}^2 [C_d - b]} \qquad [47]$$

$$\frac{\partial\eta}{\partial b} = \frac{\pi r_o \eta^2}{2a\rho Q_{exp}} \qquad [48]$$

Equation [44] was used to quantify the scatter evident in Figure 11. The solid lines represent the predicted scatter. Since the majority of the calculations are confined to this boundary, the error analysis has successfully quantified the error in the viscosity measurement. It is of interest to note that error in viscosity is a function of head, as indicated by Eq. [45].

2. *Viscosity of aluminum as a function of temperature*

Results obtained for viscosity as a function of temperature are presented in Figure 10 with viscosities determined from other studies. It is evident that values obtained from this study are significantly lower than two other studies quoted from the literature; however, results are in reasonable agreement with the theoretical approach outlined by Hirai.[3] Explanation of conventional methods to measure viscosity of melts is warranted.

3. *Viscosity measurement techniques*

Viscosity is a physical property that is related to the resistance to flow when subjected to an external force. Rotational methods used in measuring viscosity rely on the development of Couette flow that ensures a linear velocity gradient.[2] These methods use a crucible containing a melt that is rotated at a constant angular velocity. Due to the viscous nature of the liquid, motion of the liquid is induced, which exerts a torque on a cylinder placed at the center of the crucible. The viscosity is the proportionality constant relating the torque to the linear velocity gradient.

Another laminar flow configuration used in determining viscosity is the Hagen–Poiseuille law for laminar flow in pipes. In this case, a parabolic velocity profile is the result of fully developed flow in circular pipes where entrance effects are insignificant. The capillary method uses this flow pattern to measure viscosity. The time required to discharge a certain volume of fluid depends on the viscosity of the liquid.

Another group of methods are oscillatory in nature. The literature values presented in Figure 12 rely on these methods. The decreasing frequency of a submerged object that is set to oscillations is related to the viscosity of the melt.[31,32] A full description of methods used in measuring viscosity is available elsewhere.[2] The flow configurations and the methods associated with them are valid for Newtonian liquids only if the flow is laminar.

In this study, measurements are made in a turbulent regime where Reynolds numbers are in excess of 4000. The low viscosity values that were determined are still under investigation; however, the turbulent conditions at the orifice exit indicate that the laminar principle inherent to conventional measurements is not applicable under the experimental conditions described in this work.

Figure 12 illustrates that the estimation proposed by Hirai is in closer agreement with our experimental results. This calculated approach is based on quasi-crystalline theory as opposed to measurements based on laminar flow regime.[3] A word of caution is suggested when applying Hirai's calculation for comparison, as there is uncertainty to the units of molecular weight to be used in Hirai's model.[34] This could significantly alter the magnitude of the calculated viscosity.

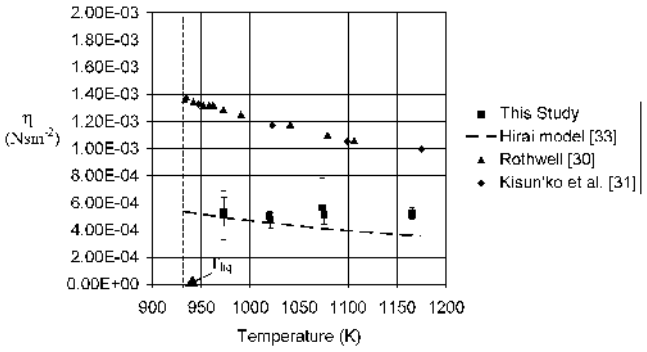

Fig. 12—Viscosity of aluminum as a function of temperature.

IV. CONCLUSIONS

A draining vessel system can be used to calculate the physical properties of liquids since surface tension, viscosity, and density are inherent in the analysis. By accurately measuring flow rate and head, these properties are determined using multiple nonlinear regression analysis. There is a statistical advantage to this technique over conventional methods because a vast quantity of data is used to calculate the properties (due to varying head and flow rate). This technique is useful for melts because of the relatively simple design of the equipment, coupled with the simultaneous measurement of all three properties. Furthermore, and unlike conventional methods, surface tension and density is determined under highly dynamic conditions in which the surface is continuously replenished.

From experiments performed with molten aluminum, the following conclusions are made.

1. Results for the surface tension of aluminum are closely related to the relationship proposed by Keene, providing validation of the technique.
2. Results for the surface tension are for aluminum having an oxidized surface and are in agreement with the relationship proposed by Keene (oxidized surface) in contrast to the higher values reported by Gourmini and Joude for an oxide-free surface.
3. Results for the density of aluminum are in reasonable approximation with values obtained in the literature, providing validation of the technique.
4. The viscosity of aluminum is significantly lower than experimental results obtained from other researchers.

A number of design issues can be considered to facilitate more accurate measurements. For instance, technology is available that electronically measures the melt head as a function of time. Independent measurements of head and cumulative mass data would reduce systematic errors in the calculation. Reducing the level of oxygen in the apparatus should be investigated to provide consistent measurements. Finally, study into the lower viscosities obtained in this study is recommended with attention focused on the turbulent characteristics of the stream. Investigation into theoretical formulations will also be undertaken to determine if there is possible agreement with results in this study. These recommendations are expected to improve upon the potential of this unique method, which is readily applicable not only to pure metals but also to alloys, slags, and molten salts.

NOMENCLATURE

A	constant in Arrhenius' formula (Pa s)
a	polynomial constant describing slope of the discharge coefficient curve (no units)
B	constant in Arrenius's formula (J/mole)
b	polynomial constant describing the y-intercept of the discharge coefficient curve (no units)
C_d	discharge coefficient (no units)
C_m	cumulative mass (kg)
ΔE	vector describing the error in experimental and calculated head values for regression analysis (m)
g	gravitational constant (m/s^2)
h	liquid head above a point of reference (m)
M	molecular weight (kg/mole)
Q	volumetric flow rate (m^3/s)
R	gas constant (8.3144 J/mol)
Re	Reynolds number (no units)
r	radius (m)
T	temperature (K)
t	time (s)
u	velocity (m/s)
Δx	vector describing change in surface tension, viscosity, or density for regression analysis
V_{exp}	mass flux of melt (kg/m^2 s)
Z	matrix of partial derivatives for regression analysis
Y	vector describing difference between experimental head and calculated head for regression analysis (m)
z	distance on z-axis (m)
δ	error in a measurement; also represents standard deviation
ε	tolerance for regression analysis (no units)
η	viscosity (Nsm^{-2})
ρ	density (kg/m^3)
σ	surface tension of liquid (N/m)

Subscripts

Al	aluminum
exp	experimental
i	sample number 'i'
j	iteration number for mutiple nonlinear regression analysis
liq	liquidus
n	sample number
o	orifice
v	vessel
η	viscosity
ρ	density
σ	surface tension

ACKNOWLEDGMENTS

The authors acknowledge the contribution of Alcoa and the NSERC Strategic Projects Program for financial support of this work.

REFERENCES

1. Y.Z. Lü, Q.D. Wang, W.J. Ding, and X.O. Zeng: *Z. Metalkd.*, 2000, vol. 91, pp. 477-82.
2. T. Iida and R.I.L. Guthrie: *The Physical Properties of Liquid Metals*, Clarendon Press, Oxford, United Kingdom, 1988, pp. 77-188.
3. M. Hirai: *Iron Steel Inst. Jpn. Int.*, 1993, vol. 33, pp. 251-58.

4. A.J. Yule and J.J. Dunkley: *Atomization of Melts: For Powder Production and Spray Deposition*, Clarendon Press, Oxford, United Kingdom, 1994, p. 17.
5. J.C. Joud and A. Passerone: *Heterogeneous Chem. Rev*., 1995, vol. 2, pp. 173-211.
6. K. Mukai and Z. Wang: *J.M. Toguri Symp.*: *Fundamentals of Metallurgical Processing*, Met. Soc. of CIM, Montreal, Canada, 2000, pp. 265-79.
7. B.J. Keene: *Int. Mater. Rev*., 1993, vol. 38, pp. 157-92.
8. G. Kaptay: *Mater. Sci. Forum*, 1991, vol. 77, pp. 315-30.
9. S.J. Roach: Master's Thesis, University of Alberta, Alberta, 2001, pp. 84-105.
10. S.J. Roach and H. Henein: *Light Metals 2001*, New Orleans, LA, 2001, TMS, Warrendale, PA, 2001, pp. 1285-1291.
11. J.R. Taylor: *An Introduction to Error Analysis: The Study of Uncertainties in Physical Measurements*, 2nd ed., University Science Books, Sausalito, CA, 1997, p. 75.
12. L. Goumiri and J.C. Joud: *Acta Metall*., vol. 30, 1982, pp. 1397-1405.
13. G. Lang: *Aluminium*, 1974, vol. 50, pp. 731-34 (in German).
14. L. Gourmiri, J.C. Joud, P. Desre, and J.M. Hicter: *Surf Sci*., 1979, vol. 83 (2), p. 471.
15. E.S. Levin, G.D. Ayushina, and P.V. Gel'd: translated from *Teplofizika Vysokika Temperature*, 1968, vol. 6 (3), pp. 432-35.
16. Y.V. Naidich and V.N. Eremenko: *Fiz. Met. Metalloved*., vol. 11 (6), p. 883 (in Russian), 1961.
17. S.I. Popel, V.N. Kozhurkov, and A.A. Zhukov: *Izv. Akad. Nauk SSSR, Met*., 1975, vol. 5, p. 69 (in Russian).
18. E.S. Levin, G.D. Ayushina, P.V. Gel'd, M.A. Ryss, and V.F. Seryii: in *Fiz. Khim. Poverkh. Yav. vys. Temp*., V.N. Eremenko, ed., Naukova Dumka., Kiev, vol. 120, 1971 (in Russian).
19. V.A. Paramanov, E.P. Karamyshev, and V.F. Ukhov: *Fiz. Khim. Poverkh. Rasp., (Coll. on Physics and Chemistry of Surface Melts)*, Metsniyereba, 1977, 155 (in Russian).
20. G.D. Ayushina, E.S. Levin, and G.D. Gel'd: *Russ. J. Phys. Chem*., 1969, vol. 43 (11), p. 1548.
21. V. de L. Davies and J.M. West: *J. Inst. Met*., 1963–64, vol. 92, p. 208.
22. C.G. Cordovilla, P. Louis, and A. Pamies: *J. Mater. Sci*., 1986, vol. 21, pp. 2787-92.
23. N.A. Bykova and V.G. Shevchenko: *Tr. Inst. Khim. Ural. Nauchn. Tsentr. Akad. Nauk SSr*., 1974, vol. 29, p. 42 (in Russian).
24. P. Laty, J.C. Joud, and P. Desré: *Surf. Sci*., vol. 69, pp. 508-20 (in French), 1977.
25. S.P. Yatsenko, V.I. Kononenko, and A.L. Sukhman: translated from *Teplofixika Vysokikh Temperatur*, 1972, vol. 10 (1), pp. 66-71.
26. E. Pelzel: *Berg Hüttenmänn. Montatsh*., 1948, vol. 93, p. 247.
27. E. Pelzel: *Berg Hüttenmänn. Montatsh*., 1949, vol. 94, p. 10.
28. N. Eustathopoulos, J.C. Joude, P. Desré, and J.M. Hicter: *J. Mater. Sci*., 1974, vol. 9, p. 1233.
29. N.A. Vatolin, O.A. Esin, V.F. Ukhov, and E.L. Dubinin: *Tr. Inst. Metall. (Sverdlovsk)*, 1969, vol. 18, p. 73 (in Russian).
30. E.I. Franses, O.A. Basaran, and C.-H. Chang: *Curr. Opinion Colloid Interface Sci*., 1996, vol. 1, pp. 296-303.
31. E. Rothwell: *JIM*, 1961–62, vol. 90, pp. 389-94.
32. V.Z. Kisun'ko, I.A. Novokhatskii, A.Z. Beloborodov, Y.B. Bychkov, and A.I. Pogorelov: *Tsvetnte Metally (Non-Ferrous)*, 1983, vol. 24 (1), pp. 84-85.
33. E.N. Andrade: *Phil. Mag*., 1934, vol. 17, p. 698.
34. M. Hirai: private communication, 2002.
35. C.J. Smithells: *Metals Reference Book*, 7th ed., Butterworths, Boston, MA, 1998, p. 14-7.